

1

## 2 **Observations of Particles at their Formation Sizes in Beijing, China**

3

4 Rohan Jayaratne<sup>1†</sup>, Buddhi Pushpawela<sup>1†</sup>, Congrong He<sup>1</sup>, Hui Li<sup>2</sup>, Jian Gao<sup>2\*</sup>, Fahe Chai<sup>2</sup>, Lidia  
5 Morawska<sup>1\*</sup>,

6

7 1 International Laboratory for Air Quality and Health, Queensland University of  
8 Technology, GPO Box 2434, Brisbane 4001, Australia.

9 2 Chinese Research Academy of Environmental Sciences, Beijing 100012, China.

10

11

12 Revised and Submitted to

13 Atmospheric Chemistry and Physics

14 May 2017

15

16

17

18 † Joint first authors.

19 \* Joint corresponding author contact details:

20 Lidia Morawska

21 Tel: (617) 3138 2616; Fax: (617) 3138 9079

22 Email: [l.morawska@qut.edu.au](mailto:l.morawska@qut.edu.au)

23 Jian Gao

24 Tel: 010 84933433; Fax: 010 84915163

25 Email: gaojian@craes.org.cn

## Abstract

26  
27  
28  
29  
30  
31  
32  
33  
34  
35  
36  
37  
38  
39  
40  
41  
42  
43  
44  
45  
46  
47  
48  
49  
50  
51

New particle formation (NPF) has been observed in many highly polluted environments of South-East Asia, including Beijing, where the extent of its contribution to intense haze events is still an open question. Estimated characteristics of NPF events, such as their starting times and formation and growth rates of particles, are more accurate when the detection range of particles extends to smaller sizes. In order to understand the very first steps of particle formation, we used a neutral cluster and air ion spectrometer (NAIS) to investigate particle characteristics at sizes exactly where atmospheric nucleation and cluster activity occurs. Observations over a continuous three-month period in Beijing showed 26 NPF events. These events generally coincided with periods with relatively clean air when the wind direction was from the less-industrialized north. No NPF were observed when the daily mean  $PM_{2.5}$  concentration exceeded  $43 \mu\text{g m}^{-3}$ , which was the upper threshold for particle formation in Beijing. The fraction of particles that are charged in the size range 2-42 nm was normally about 15%. However, this fraction increased to 20-30% during haze events and decreased to below 10% during NPF events. With the NAIS, we determined the starting times of NPF very precisely to a greater accuracy than has been possible in Beijing before and provided a temporal distribution of NPF events with a maximum at about 8.30 am. Particle formation rates varied between  $12\text{-}38 \text{ cm}^{-3} \text{ s}^{-1}$ . Particle growth rates were estimated to be in the range  $0.5\text{-}9.0 \text{ nm h}^{-1}$ . These results are more reliable than previous studies in Beijing as the measurements were conducted for the first time at the exact sizes where clusters form into particles and provide useful insight into the formation of haze events.

**Keywords:** New particle formation, secondary particles, nucleation, haze events

---

## 52 1. Introduction

53

54 Particles in the atmosphere may be classified into two types depending on their origin. Primary  
55 particles are directly emitted by a source while secondary particles are formed through a secondary  
56 process by the homogeneous condensation of gaseous precursors. This is known as new particle  
57 formation (NPF) and has been observed in many parts of the world in many different types of  
58 environments (Curtius, 2006;Kulmala et al., 2005;Kulmala et al., 2004;Zhang et al., 2011). NPF is a  
59 complicated process where molecular clusters come together to form particles at a size of about 1.6  
60 nm (Kulmala et al., 2004). Generally, it is favoured by clean air conditions where the particle number  
61 concentration (PNC) in the atmosphere is low, resulting in a lower particle surface available for the  
62 condensation of gases, leading to an increase of the supersaturation in the air enhancing  
63 homogeneous condensation of the gaseous species (Kulmala et al., 2005;Wu et al., 2011) and,  
64 therefore, NPF is less frequent in polluted environments. However, if the gaseous precursor  
65 concentration is high enough, NPF may occur at even higher particle concentrations (Kulmala et al.,  
66 2005;Wu et al., 2011). Jayaratne et al. (2015) showed that in the relatively clean environment of  
67 Brisbane, Australia, NPF do not occur when the ambient PM<sub>10</sub> concentration exceeds about 20 µg  
68 m<sup>-3</sup>. However, NPF have been commonly observed in more polluted environments like Beijing  
69 (Kulmama et al., 2016) and Shanghai (Xiao et al., 2015) in China. Kulmala et al. (2017) proposed that  
70 the survival efficiency of clusters to form particles is determined by the two key parameters –  
71 condensation sink (CS) and cluster growth rate (GR). They defined a dimensionless survival  
72 parameter, P, equal to the ratio  $(CS/10^{-4} s^{-1})/(GR/nm h^{-1})$  and showed that P needs to be smaller  
73 than about 50 for a notable NPF to take place. However, it was noted that NPF occurred frequently  
74 in megacities in China where the calculated P values were much higher. They hypothesized that this  
75 discrepancy may be explained if the molecular clusters were being scavenged less effectively than  
76 expected based on their collision rates with pre-existing particles or if they grew much faster in size  
77 than our current understanding allows.

78 The study of the formation and characteristics of NPF events in Beijing is important because of its  
79 possible influence on severe haze episodes (Guo et al., 2014;Huang et al., 2014). Such haze events  
80 not only give rise to poor visibility but are responsible for sharp increases in respiratory problems  
81 amongst the large population that is exposed. In particular, Beijing experienced severe haze  
82 episodes during November and December, 2015. Daily maximum PM<sub>2.5</sub> values in the city exceeded  
83 500 µg m<sup>-3</sup> on no less than six days during the month of December, prompting two official air  
84 pollution 'red alerts' to be issued (Xue et al., 2016). Close examination of the haze events  
85 demonstrate that they occur in cycles of a few days and generally coincide with winds blowing from  
86 the more polluted regions south of the city (Guo et al., 2014;Wu et al., 2007). Particulate matter  
87 concentrations are observed to drop significantly when the winds change to a northerly direction,  
88 bringing cleaner air into the city, which is when NPF events generally occur (Guo et al., 2014;Huang  
89 et al., 2014).

90

91 The earliest study of NPF using a TSI scanning mobility particle sizer (SMPS) in Beijing was carried out  
92 by Wehner et al. (2004). They observed NPF on 25 out of 45 days of measurement, and on each of  
93 these days the PNC exceeded 10<sup>5</sup> cm<sup>-3</sup>. Subsequent studies using the SMPS were carried out by Wu  
94 et al. (2007) who showed that NPFs were observed on 50%, 20%, 35% and 45% of days during the  
95 spring, summer, fall and winter seasons, respectively. Yue et al. (2010) investigated 12 NPF events  
96 and showed that sulphuric acid and ammonia accounted for about 45% of the growth rate, with the  
97 balance being due to organic species. Guo et al. (2014) conducted a detailed analysis over a two-  
98 month period during the fall of 2013 and showed that NPF events occurred in a clear periodic cycle  
99 of about 4-7 days coinciding with northerly winds bringing cleaner air into the city. The average  
100 PM<sub>2.5</sub> values when the wind was from the north and when it was from the south were 35 and 114 µg  
101 m<sup>-3</sup>, respectively. The average PM<sub>2.5</sub> (and PNC) values during and outside the NPF periods were less  
102 than 50 µg m<sup>-3</sup> (greater than 2 x 10<sup>5</sup> cm<sup>-3</sup>) and several hundred µg m<sup>-3</sup> (5 x 10<sup>4</sup> cm<sup>-3</sup>), respectively.  
103 Pollution also originates from within the city – from motor vehicle emissions and industrial sources.

104 In general, airborne gaseous pollutants in Beijing and other urban regions in China are mainly  
105 volatile organic compounds (VOC) and oxides of nitrogen ( $\text{NO}_x$ ) from local transportation and  
106 sulphur dioxide ( $\text{SO}_2$ ) from regional industrial sources (Wang et al., 2009; Yue et al., 2010). However,  
107 Guo et al. (2014) showed that the nucleation and growth processes occurred on a regional scale,  
108 over several hundred km, with the effect of local sources such as motor vehicle emissions being  
109 insignificant. A good summary of the studies conducted since 2004 in Beijing may be found in Zhibin  
110 et al. (2013) and Kulmama et al. (2016).

111

112 All these previous studies in Beijing have been carried out using the SMPS. The SMPS is a good tool  
113 to determine the PNC and size distribution down to a minimum particle size of about 3 nm, although  
114 the efficiency of detection falls off below about 10 nm. Thus, an event where aerosols in the size  
115 range 3-10 nm emitted on-site as primary particles or entrained from a distant location that  
116 continue to grow to larger sizes may be mistaken for particle formation at that monitoring site. The  
117 SMPS is also not able to identify the exact time period during which particle formation occurs. An  
118 instrument that can detect particles at smaller sizes is the neutral cluster and air ion spectrometer  
119 (NAIS) from Airel Ltd. The NAIS is specifically designed to monitor NPF as it can detect particles down  
120 to their actual formation sizes (Manninen et al., 2016; Manninen et al., 2009; Mirme et al., 2007). In  
121 this paper, we present the first results of using a NAIS in Beijing over the course of three months,  
122 two months with intense haze and very few NPF events, and the other including several days with  
123 NPF. We will investigate the characteristics of the NPF events and the conditions that gave rise to  
124 them. As the measurements included the sizes at which particles formed, the results provide more  
125 reliable information of such parameters as the starting times, growth rates and formation rates of  
126 particles than has been possible in the past.

127

128        **2. Methods**

129

130        **2.1 Instrumentation**

131        The NAIS is an improved version of the air ion spectrometer (AIS) which was developed by Airel Ltd  
132        (Mirme et al., 2007). In both instruments, the sample air is split equally into each of two separate  
133        cylindrical spectrometer columns, one of each polarity. At the inlet to each column, a unipolar  
134        corona wire diffusion charger of the same polarity as the central electrode in the column brings the  
135        particles to an equilibrium charge distribution. They are then classified by a differential mobility  
136        analyser where the outer electrodes consist of 21 insulated sections or rings, each with its own  
137        electrometer. The charged particles in the air flow are repelled by the central electrode which has a  
138        tapered cross-section and collected by the rings. The electric field between the central electrode and  
139        the rings is fixed by the voltage on the inner electrode and the gap between the inner and outer  
140        electrodes so that only particles in a given mobility range may be collected by each ring. In this way,  
141        the instrument can separate particles into 21 mobility or size bins. A refinement in the NAIS over the  
142        AIS is that it uses controlled charging to measure the concentration of charged particles in addition  
143        to the total PNC in each size range. This is done by switching the voltage off on the corona charger  
144        during one part of the measurement cycle. Thus, the NAIS can measure both charged and neutral  
145        particles separately. The mobility range of the instrument is  $3.16\text{-}0.001\text{ cm}^2\text{ V}^{-1}\text{ s}^{-1}$  which corresponds  
146        to a mobility diameter range of 0.8-42 nm. However, Asmi et al. (2009), Manninen et al. (2011) and  
147        Manninen et al. (2016) have pointed out that the lowest detection limit for the NAIS in the particle  
148        mode is about 2.0 nm owing to the presence of corona-generated ions; at sizes smaller than 2.0 nm,  
149        the NAIS cannot reliably distinguish between charged and neutral particles. Therefore, Manninen et  
150        al. (2011) specified the lowest detection limit of the NAIS to be 1.6 and 1.7 nm for negative and  
151        positive ions, respectively, and 2.0 nm for neutral particles. Therefore, in this study, we will restrict  
152        our observations to the particle size range 2.0-42 nm. A good description of the detailed operation  
153        of the NAIS may be found in Manninen et al. (2016). In this study, we set the NAIS to a measurement

154 cycle of 5 min consisting of 2 min each for charged and neutral particles with an offset period of 1  
155 min. Thus, a PNC and charged particle concentration reading were obtained in real time once every 5  
156 min.

157

158 The larger size PNC was monitored with an SMPS. The instrument was set to scan up and retrace  
159 times of 120 and 15 s respectively. The aerosol and sheath flow rates were 0.3 and 3.0 lpm,  
160 respectively. Size distributions were determined in 107 bins in the size range 14 to 673 nm. A  
161 complete size distribution record was obtained every 5 min.  $PM_{2.5}$  concentrations were monitored  
162 with a tapered element oscillating monitor (TEOM) and recorded as hourly average values.

163

## 164 **2.2 Study Design**

165 The NAIS and SMPS were set up within a room on the roof of the Chinese Research in Atmospheric  
166 and Environmental Sciences (CRAES) Building in Beiyuan, Beijing, on the 28 October 2015 and  
167 monitoring was conducted continuously until 31 January 2016. This comprised 96 days including  
168 several episodes of very high pollution or haze days when the  $PM_{2.5}$  in Beijing exceeded 100-200  $\mu g$   
169  $m^{-3}$ . Data was lost on nine days owing to various problems such as the loss of power, software  
170 malfunction and a blocked filter during a haze event. Air was sampled through a straight steel pipe  
171 of diameter 4 cm protruding vertically through the roof of the building. Meteorological parameters,  
172 including the wind speed, wind direction, air temperature and relative humidity were monitored and  
173 recorded hourly over the course of the study period.

174

## 175 **2.3 Analysis**

176

### 177 **2.3.1 Identification of NPF events**

178 The NAIS provided spectragrams showing the neutral and charged particle number size distributions  
179 in real time with the concentrations shown in colour contours. The neutral and charged PNCs were

180 also provided in real time at 5 min intervals. NPF events were identified using the method proposed  
181 by Zhang et al. (2004). We calculated the rate of change of PNC,  $dN/dt$ , where  $N$  is the number of  
182 particles in the size range 2.0 -10.0 nm. Events with  $N > 10,000 \text{ cm}^{-3}$  for at least 1 hour and  $dN/dt$   
183  $>15,000 \text{ cm}^{-3}\text{h}^{-1}$  were classified as NPF events. These events generally exhibited a ‘banana shape’ in  
184 the spectragrams. A day on which there was at least one NPF event as defined above was termed an  
185 “NPF day”. A day where the above criteria were not fulfilled were classified as a “non-event” day. A  
186 “haze day” was defined as a day when the 24-hour average  $\text{PM}_{2.5}$  concentration exceeded  $75 \mu\text{g m}^{-3}$   
187 - the national air quality standard in China. A day on which there was neither NPF or haze was  
188 defined as a “normal day”. NPF events are characterised by sharp increases in the intermediate size  
189 range. The starting times of an event was determined by using the time of sudden increase in PNC in  
190 the size range 2.0 – 10.0 nm.

191

### 192 **2.3.2 Condensation sink (CS) and coagulation sink (CoagS)**

193 The condensation sink of particles is defined as (Dal Maso et al., 2002; Dal Maso et al., 2005; Kulmala  
194 et al., 2012; Lehtinen et al., 2003; Salma et al., 2011)

$$195 \quad CS = 2 \pi D \sum_i \beta_m (d_{p,i}) d_{p,i} N_i$$

196 (1)

197 where  $D$  is the diffusion coefficient of the condensing vapour and  $\beta_m$  is the transition correction  
198 factor for mass flux.  $d_{p,i}$  and  $N_i$  are the diameter and the number concentration of particles in the size  
199 bin  $i$  respectively. The unit of CS is  $\text{s}^{-1}$ .

200 It is now well established that sulfuric acid is the key precursor gas in nucleation, although low  
201 vapour pressure organics may contribute to the subsequent aerosol growth (Curtius, 2006). Sulfuric  
202 acid has a low vapour pressure which is reduced further in the presence of water. When produced



203 from SO<sub>2</sub> in the gas phase, it is easily supersaturated and begins to condense. Moreover, most of the  
 204 particles in the atmosphere are in the kinetic regime (smaller than 0.01 μm)(Seinfeld and Pandis,  
 205 2006a). In this regime, condensation is directly proportional to the RMS speed of the molecules. The  
 206 RMS speed is inversely proportional to the square root of the molecular weight of the molecule.  
 207 Thus, a sulfuric acid molecule, with a molecular weight of 98 g mol<sup>-1</sup>, has an RMS speed that is about  
 208 30% higher than a typical organic gas molecule with a molecular weight of about 200 g mol<sup>-1</sup>, Thus,  
 209 condensation of sulfuric acid will occur much more readily than organic molecules. Studies in Beijing  
 210 have confirmed that NPF is more likely to occur in a sulfur-rich environment than in one that is  
 211 sulfur-poor ((Yue et al., 2010;Guo et al., 2014;Wu et al., 2007)). Wu et al. (2007) also assumed that  
 212 sulfuric acid was the main condensable vapour in determining the particle formation rates during  
 213 NPF events in Beijing.

214 Therefore, assuming that the main condensing vapour is sulphuric acid, we estimated the diffusion  
 215 coefficient for condensing vapour using the expression

$$216 \quad D = 5.0032 * 10^{-6} + 1.04 * 10^{-8}T + 1.64 * 10^{-11}T^2 - 1.566 * 10^{-14}T^3 \quad (2)$$

217 where  $D$  has the units of m<sup>2</sup> s<sup>-1</sup> and where the temperature  $T$  is in Kelvin (Jeong, 2009).

218 The transition correction factor,  $\beta_m$ , was calculated using the Fuchs-Sutugin expression (Fuchs and  
 219 Sutugin, 1971)

$$220 \quad \beta_m = \frac{Kn + 1}{1 + (\frac{4}{3\alpha} + 0.337)Kn + (\frac{4}{3\alpha})Kn^2} \quad (3)$$

221 where

$$222 \quad Kn = \frac{2\lambda}{d_p} \quad \text{and} \quad 0 \leq \alpha \leq 1 .$$

223

224 Here,  $Kn$ , the Knudsen number, describes the nature of the suspending vapour relative to the  
225 particle,  $\lambda$  is the mean free path of a suspending vapour molecule and  $d_p$  is the diameter of the  
226 particle (Seinfeld and Pandis, 2006b). The mass accommodation coefficient (sticking coefficient)  $\alpha$   
227 describes the probability of a vapour molecule sticking to the surface of a particle during vapour-  
228 particle interactions (Seinfeld and Pandis, 2006b). In this study, we assumed  $\alpha = 1$ .

229

230 The relationship between the condensation sink and coagulation sink is given by Lehtinen et al.  
231 (2007) as

$$CoagS_{d_p} = CS \cdot \left( \frac{d_p}{0.71} \right)^m$$

232 (4)

233 where the exponent  $m$  varies in the range -1.75 to -1.5 with a mean value -1.7 and the value 0.71 is  
234 the diameter of a hydrated sulphuric acid molecule. The unit of CoagS is  $s^{-1}$ .

235

236 In order to calculate the CS, we used the PNC obtained from the SMPS in the 107 size bins in the  
237 range 14-673 nm and from the NAIS in 8 size bins in the range 2-14 nm. The mean temperature in  
238 Beijing during the period of observation was close to 0°C. The value of  $D$  calculated using equation  
239 (2) at temperature  $T = 273$  K was  $0.087 \text{ cm}^2 \text{ s}^{-1}$  which is in good agreement with the values given in  
240 the literature (Brus et al. 2016;Eisele and Hanson, 2000). The values used for the exponent  $m$  was -  
241 1.7 (Dal Maso et al., 2008) and  $\lambda = 108$  nm (Massman, 1998).

242

243

244

245

246 **2.3.3 Particle formation rate**

247 Particle formation or nucleation occurs from thermodynamically stable clusters in the size range 1.0-  
248 2.0 nm (Kulmala et al., 2007). The formation rate may be estimated from the number of particles in  
249 the smallest size bin, usually 2-3 nm in the NAIS.

250 The formation rate of particles is defined as

$$J_{d_p} = \frac{dN_{d_p}}{dt} + CoagS_{d_p} \cdot N_{d_p} + \left( \frac{GR}{\Delta d_p} \right) N_{d_p}$$

251 (5)

252 where  $N_{d_p}$  is the number concentration of particles in the size range  $d_p$  and  $(d_p + \Delta d_p)$  respectively  
253 (Kulmala et al., 2012). In this study, we used the values  $d_p = 2$  nm and  $\Delta d_p = 1$  nm, corresponding to  
254 the size range 2-3 nm.  $CoagS_{d_p}$  represents the loss of the particles due to coagulation in the size  
255 range 2-3 nm, calculated from equation (4) with  $d_p = 2$  nm, and  $GR$  is the growth rate of particles.  
256 The unit of formation rate is  $\text{cm}^{-3} \text{s}^{-1}$ .

257

258 **2.3.4 Particle growth rate (GR)**

259 During an NPF event, the growth rate of particles was defined by Kulmala et al. (2012) as

$$GR = \frac{dd_p}{dt} = \frac{d_{p2} - d_{p1}}{t_2 - t_1}$$

260 (6)

261 where  $d_{p2}$  and  $d_{p1}$  are the diameters of particles at times  $t_2$  and  $t_1$ , respectively. This was calculated  
262 by the maximum concentration method as described in Kulmala et al. (2012) by examining the time  
263 of maximum PNC at each particle size during an NPF event. First, we exported the number  
264 concentrations of particles obtained from the NAIS in 14 bins in the size range 2.0 – 42.0 nm. Next,

265 we selected the time of maximum concentrations during each NPF event for each particle size bin.  
266 Finally, we calculated the growth rate using the slope of the best-fitted line on the graph of median  
267 diameter of particle in each size bin vs. the time of maximum concentration. The unit of GR is  $\text{nm h}^{-1}$ .

268

### 269 **3. Results and Discussion**

270

#### 271 **3.1 Distribution of NPF events**

272 During the entire period of measurement, the NAIS yielded 87 complete days of data, the remaining  
273 9 days being affected by instrument faults, generally due to power fluctuations. November and  
274 December 2015 were particularly prone to high pollution events in Beijing. The daily average  $\text{PM}_{2.5}$   
275 concentration exceeded the recommended maximum of  $50 \mu\text{g m}^{-3}$  in Beijing on 47 days during this  
276 two-month period. The maximum daily average was  $448 \mu\text{g m}^{-3}$  and this occurred on 1<sup>st</sup> December.  
277 Owing to the high condensation sink on polluted days, there were relatively few NPF days during  
278 these two months. There was a relative improvement of air quality after 4<sup>th</sup> January and this lasted  
279 until 31<sup>st</sup> January - the end of the monitoring period, during which time, the daily average exceeded  
280  $100 \mu\text{g m}^{-3}$  on only four days. Enhanced  $\text{PM}_{2.5}$  concentrations ( $> 50 \mu\text{g m}^{-3}$ ) were observed on 15  
281 days in January. These days occurred in groups and we could identify five such distinct periods  
282 during January. No NPF events were observed during these 15 days; however, several NPF events  
283 were observed on the other days during the intervening periods. A summary of the observational  
284 days, together with the number of days on which data were available and NPF events were  
285 observed, are shown in Table 1. Column 3 shows the numbers of days on which complete 24-hour  
286 data were obtained. We note that during the 56 such days between 27<sup>th</sup> October and 31<sup>st</sup> December,  
287 NPF events were observed on just 10 days, whereas during the 31 days in January 2016, NPF events  
288 took place on 16 days. The near equal division between NPF days and no-NPF days in January  
289 provided an ideal data set to compare the parameters and conditions on these two types of days.

290 The difference between November/December and January had a clear dependence on the  $PM_{2.5}$   
291 concentrations. Figure 1 gives a summary of the days on which NPF events were observed.

292

### 293 **3.2 Relationship between NPF events and $PM_{2.5}$ concentration**

294 In Fig 2, we take a closer look at the January data, together with the respective mean daily  $PM_{2.5}$   
295 concentrations. It is apparent that there were five distinct groups of NPF days in January. These are  
296 labelled in 2(b). In the NAIS spectragram, shown in 2(a), the 16 NPF events are clearly observed with  
297 the characteristic 'banana' shapes compressed into near-vertical bands extending up from the  
298 smallest sizes. The five groups from left to right consist of 5, 3, 2, 5 and 1 NPF events, respectively  
299 (Figs 2(a and b)). These groups are separated by time periods when no NPFs were observed. The  
300  $PM_{2.5}$  values are clearly lower on NPF days than on the other days with mean daily values of  $18 \mu g m^{-3}$   
301 and  $120 \mu g m^{-3}$ , respectively. A Student's t-test showed that the difference in mean daily  $PM_{2.5}$   
302 values between NPF days and the other days was statistically significant at the confidence level of  
303 95%. The corresponding difference was even more significant when considering the entire  
304 monitoring period where the mean daily values of  $PM_{2.5}$  on NPF days and the other days were  $21 \mu g$   
305  $m^{-3}$  and  $143 \mu g m^{-3}$ , respectively. Figure 2(c) shows the corresponding mean daily PNC. While the  
306 PNC within each group showed a greater fluctuation than the  $PM_{2.5}$ , the PNC on NPF days was  
307 significantly higher than on non-NPF days. Therefore, although the PM is higher on haze days than  
308 on NPF days, the t-tests again showed that the PNC was significantly lower on haze days than on NPF  
309 days. This is explicable in terms of the particle size. Particles are significantly larger on haze days  
310 than on clean days when NPF events are likely to occur.

311

312 In Fig 3, we plot the daily mean PNC against the daily mean  $PM_{2.5}$  for the 31 days in January. The days  
313 with NPF and the days with no NPF events clearly fall into two distinct groups according to the daily  
314 mean  $PM_{2.5}$  values. Pre-existing particles entering the region with the winds from the south will also  
315 increase the condensation sink, further reducing the likelihood of NPF.

316 No NPF events were observed on a day when the mean  $PM_{2.5}$  value exceeded  $43 \mu\text{g m}^{-3}$ . There is  
317 some minor overlap in the PNC values on the two types of days but this is primarily because they are  
318 daily averages. When we consider the average PNC values during the NPF events alone, a t-test  
319 showed that they are significantly higher than at other days and times. However, we do see that, on  
320 haze days, the daily average PNC does not exceed  $8.5 \times 10^4 \text{ cm}^{-3}$ .

321

### 322 **3.3 Relationship between NPF events and wind direction**

323 Previous studies have shown that the wind direction played an important role in determining the  
324  $PM_{2.5}$  concentration in Beijing (Guo et al., 2014). Again, we look at the month of January, as it  
325 provided an almost equal number of NPF days and other days and was, therefore, ideal to compare  
326 the wind direction on the two types of days. Figure 4 shows the wind direction roses for both NPF  
327 days and other days during January. The frequencies are given as percentages of time when the  
328 wind was from a given direction. There is a clear difference between the two sets of days with a  
329 strong correlation between the NPF days and the wind direction. NPF events clearly occurred on  
330 days when the wind direction was predominantly from the NW, while it was more equally  
331 distributed with a greater likelihood of arriving from the S and E during the haze days when there  
332 were no NPF events. The frequencies in the sector between NW ( $315^\circ$ ) and N ( $0^\circ$ ) on NPF days and  
333 other days were 68 % and 11 %, respectively. Air from the north of Beijing is usually cleaner than  
334 that from the more industrialized south of the city (Guo et al., 2014). Clean periods are characterised  
335 by decreased condensation sinks that promote NPF. Winds from the south bring a copious supply of  
336 freshly available gaseous precursors that should give rise to particle formation. However, the  
337 absence of NPF events during these times suggests that the wind is also carrying a large supply of  
338 particles that reduce the gaseous supersaturations required for particle formation. Thus, the  
339 observed haze events are unlikely to be caused by in-situ new particle formation and more likely to  
340 be due to particles carried by the wind into the city or being prevented from escaping due to  
341 temperature inversions in the atmosphere.

342

### 343 **3.4 Charged particles**

344 Next, we look at the behaviour of charged particles, with particular attention to NPF events and haze  
345 events. In order to compare and contrast the characteristics of these particles, we selected a period  
346 of four days, comprising two haze days that were immediately followed by two NPF days. Figure 5  
347 shows the time series of the concentration of total and charged particles observed over this four-day  
348 period from November 30 to December 3. The upper curve represents the total PNC while the lower  
349 curve gives the charged PNC. The difference between the two curves gives the neutral PNC. The  
350 conditions during the two types of events could be compared during this period as intense haze was  
351 observed on the first two days (Nov 30 and Dec 1) while, following a change of wind direction near  
352 midnight on the 1 December, two strong NPF events took place on the next two days (Dec 2 and 3).

353 A summary of the neutral and charged PNC during the various stages over the entire period of  
354 observation are presented in Table 2. Also shown are the percentage numbers of all particles that  
355 were found to be charged. NPF events and NPF days are defined in section 2.3.1. A haze day was  
356 defined as a day when the 24-hour average  $PM_{2.5}$  concentration exceeded  $75 \mu g m^{-3}$  - the national air  
357 quality standard in China. A day that met neither of these criteria was defined as a 'normal day'.  
358 Thus, by our ad-hoc definition, a normal day had a daily average  $PM_{2.5}$  concentration in the range 43-  
359  $75 \mu g m^{-3}$ , since no NPF events were observed on days when the average  $PM_{2.5}$  concentration was  
360 greater than  $43 \mu g m^{-3}$ . The duration of the various events affected the daily values while the  
361 conditions during the events affected their peak number concentrations. The values shown are the  
362 means of the average  $PM_{2.5}$  concentrations over all the 24-hour days. The daily mean values varied  
363 from day to day, especially on days with NPF events or haze events mainly due to the different  
364 durations of these events. We estimated the standard deviation about these mean values to be 20%.  
365 On a normal day, around 15% of the particles larger than 2 nm are charged. The fraction that is  
366 charged decreases significantly during an NPF event. This is consistent with our observations in  
367 Brisbane (Jayaratne et al., 2016) and may be attributed to the rapid increase in particle number and

368 the associated coagulation. On the other hand, during a haze event, the percentage of particles  
369 charged increases to a value between 20% and 30%. These observations are consistent with the PNC  
370 and particle sizes and the equilibrium distribution of charge on particles. NPF are characterised by  
371 large numbers of small particles while the SMPS and TEOM show that haze events comprise much  
372 larger particles. The amount of charge that a particle can hold and the fraction of particles that are  
373 charged in equilibrium both increase with particle size, so it is not unexpected to find that a larger  
374 percentage of particles are charged during the haze events.

375

### 376 **3.5 Particle formation times**

377 All except one of the 26 NPF events during the period of observation began between 7:30 am and  
378 10:00 am. The mean time was 8:45 am. This result is in agreement with Wu et al. (2007) who, using  
379 an SMPS, reported that NPF events during clean air periods in November, December and January  
380 generally started between 7:00 am and 10:00 am. Figure 6 shows the temporal distribution of the  
381 start times of the NPF events, classified into 30 minute bins. The most likely time for an NPF event to  
382 begin was between 8:00 and 8:30 am. This time coincides with the morning rush hour traffic when  
383 the production rate of gaseous precursors is generally at a maximum. Sunrise in Beijing in  
384 December/January is at about 7.30 am.

385

386 Figure 7 shows the NAIS spectragram of the strong NPF event that occurred on 29<sup>th</sup> October 2015.  
387 The spectragram shows a clear banana profile which levels off at about 20 nm. The PNC in this event  
388 was relatively high, exceeding  $1.6 \times 10^5 \text{ cm}^{-3}$  near 11:00 am. The  $\text{PM}_{2.5}$  concentration remained  
389 between  $12$  and  $16 \mu\text{g m}^{-3}$  right through this event. The markers shown on this figure are the median  
390 sizes of particles at each time. It can be observed in the spectragram that particle formation began  
391 at around 09:00 h. However, previous studies in Beijing have not been able to measure particles  
392 smaller than 3 nm. In Fig 7, if we truncate the lower particle size margin to 3 nm, the starting time of  
393 the NPF event appears later than it actually is, approximately at 9:30 am. In other NPF spectragrams,



394 we see this difference being as much as 1.0 to 1.5 h depending on the initial growth rate. Thus, we  
395 conclude that the starting times that we have derived (Fig 6) are more accurate than has been  
396 obtained in the past. This will also affect the estimated growth rates of particles during NPF events  
397 as we shall show in the next section.

398

### 399 **3.6 Condensation sink**

400 The condensation sinks were calculated during NPF events assuming the growth to be due to sulfuric  
401 acid and using the SMPS and NAIS data and the equations given in the methods section. The mean  
402 value of the condensation sink was  $4.2 \times 10^{-3} \text{ s}^{-1}$ . This value is somewhat smaller than that reported by  
403 Wu et al. (2007) ( $1.4 \times 10^{-2} \text{ s}^{-1}$ ) and Wu et al. (2011) ( $1 \times 10^{-2} \text{ s}^{-1}$ ) but within the range of  $0 - 5 \times 10^{-2} \text{ s}^{-1}$   
404 reported in all NPF events between 2004 to 2008 in Beijing by Zhibin et al. (2013). The value of the  
405 condensation sink during NPF events ( $0.004 \text{ s}^{-1}$ ) was not significantly different to the corresponding  
406 average values during other times on NPF days and on normal days with no NPF ( $0.006 \text{ s}^{-1}$ ).  
407 However, the mean condensation sink on haze days ( $0.060 \text{ s}^{-1}$ ) was significantly higher than both  
408 these values.

409

### 410 **3.7 Particle formation rate**

411

412 Using our value of the CS, we calculated the mean value of the coagulation sink using equation (4)  
413 for 2 nm particles during an NPF event to be  $7.2 \times 10^{-4} \text{ s}^{-1}$ . Previous studies in Beijing have not been  
414 able to determine this value at 2 nm. The value reported for 3 nm particles for NPF events in Beijing  
415 by Wu et al. (2011) was  $9.9 \times 10^{-4} \text{ s}^{-1}$ , which is close to our value at 2 nm. Using our value of the  
416 coagulation sink in equation (5), we calculated the formation rate of particles in the smallest particle  
417 size bin 2-3 nm. At these times, the rate of increase of particles in this size bin ranged from about  
418  $5.0 \times 10^3$  to  $1.5 \times 10^4 \text{ cm}^{-3} \text{ h}^{-1}$ . The resulting formation rates varied between 12 and  $38 \text{ cm}^{-3} \text{ s}^{-1}$ , with a  
419 mean of  $26 \text{ cm}^{-3} \text{ s}^{-1}$ . Previous estimates in Beijing did not have the benefit of the PNC information in

420 the 2-3 nm size bin. Wu et al. (2007) calculated the formation rate in the wider size bin of 3-10 nm  
421 and arrived at a value in the range  $3.3\text{-}81.4\text{ cm}^{-3}\text{ s}^{-1}$  with a mean of  $22.3\text{ cm}^{-3}\text{ s}^{-1}$ . Yue et al. (2010)  
422 studied 12 NPF events in Beijing and derived a formation rate in the range  $2\text{-}13\text{ cm}^{-3}\text{ s}^{-1}$  and showed  
423 that the formation rate was directly proportional to the sulfuric acid concentration. They did not  
424 specify the size range used in this calculation but the smallest detectable particle size of the  
425 instrument used was 3 nm. These values may be compared with that found by Yu et al. (2016) in the  
426 urban atmosphere of Nanjing, China. They studied eight NPF events using a nano-condensation  
427 nucleus counter system capable of measuring particle size distributions down to 1.4 nm and  
428 estimated initial and peak particle formation rates of  $2.1\times 10^2$  and  $2.5\times 10^3\text{ cm}^{-3}\text{ s}^{-1}$ , respectively. The  
429 formation rates showed good linear correlation with a sulfuric acid proxy.

430

### 431 **3.8 Particle growth rate**

432

433 In the NPF event shown in Fig 7, the particle growth rate in the size range 2-10 nm during the entire  
434 event (between 9:00 and 11:00 am) estimated from equation (6) was  $4.8\text{ nm h}^{-1}$ . Although the PNC  
435 reached very high values, the particles did not grow much larger than about 30 nm, suggesting that  
436 the high condensation sink was restricting the precursor gas concentration in the atmosphere. The  
437 growth rate of all the NPFs observed ranged from  $0.5$  to  $9.0\text{ nm h}^{-1}$  with a mean value of  $3.5\text{ nm h}^{-1}$ .  
438 Previous estimates of the growth rate during NPF using the SMPS have yielded mean values of  $1.0$   
439  $\text{nm h}^{-1}$  (Wehner et al., 2004) and  $1.8\text{ nm h}^{-1}$  (Wu et al., 2007)., 2007). Zhibin et al. (2013) determined  
440 the growth rates of a number of NPFs in Beijing over a 4-year period and reported a range of  $0.1$  to  
441  $10\text{ nm h}^{-1}$  with a mean of  $3.0\text{ nm h}^{-1}$  which is in close agreement with our value. In contrast, Yu et al  
442 (2016) reported an exceptionally high local maximum growth rate of  $25\text{ nm h}^{-1}$  in Nanjing, China. Our  
443 values of CS and GR give a cluster survival parameter  $P = 12$  (Kulmala et al., 2017). This value is  
444 significantly lower than the maximum value of 50 that was specified as a condition for NPF.

445

446 **4 Summary and Conclusions**

447 We monitored charged and neutral PNC over a continuous three-month period for the first time in  
448 Beijing. The results showed 26 NPF events. No NPF were observed when the daily mean PM<sub>2.5</sub>  
449 concentration exceeded 43 µg m<sup>-3</sup>.

450 A summary of the main parameters determined are shown in Table 3.

451 This is the first study of NPF in the particle size range below 3 nm in Beijing. This enables the  
452 derivation of more relevant and accurate estimates of parameters, such as the times of formation  
453 and growth and formation rates, than has been possible before.

454 The results show the following features of NPF events in Beijing:

- 455 • NPF events occur during clean air episodes when the wind direction is from the north of the  
456 city.
- 457 • We have provided the first temporal distribution chart of NPF events in Beijing which shows  
458 that all but one of the 26 events began between 7:30 and 10:00 am.
- 459 • The main characteristics of the particles in the NPF events are presented in Table 3.
- 460 • The fraction of particles that are charged was normally about 15%. This fraction increased to  
461 20-30% during haze events and decreased to below 10% during NPF events.

462

463

464 **Acknowledgements**

465 This project was supported by the Australia-China Centre for Air Quality Science and Management.,  
466 the National Natural Science Foundation of China (Grant No 41375132, 91544226), and the Special  
467 Funds for Research on Public Welfares of the Ministry of Environmental Protection of China  
468 (201409003)

469

## References

- 470  
471
- 472 Asmi, E., Sipilä, M., Manninen, H., Vanhanen, J., Lehtipalo, K., Gagné, S., Neitola, K., Mirme, A.,  
473 Mirme, S., and Tamm, E.: Results of the first air ion spectrometer calibration and intercomparison  
474 workshop, *Atmospheric Chemistry and Physics*, 9, 141-154, 2009.
- 475 Brus, D., Skrabalova, L., Herrmann, E., Olenius, T., Travnickova, T., and Merikanto, J.: Temperature-  
476 dependent diffusion coefficient of H<sub>2</sub>SO<sub>4</sub> in air: laboratory measurements using laminar flow  
477 technique, *Atmos. Chem. Phys. Discuss.*, 2016, 1-26, 10.5194/acp-2016-398, 2016.
- 478 Curtius, J.: Nucleation of atmospheric aerosol particles, *Comptes Rendus Physique*, 7, 1027-1045,  
479 2006.
- 480 Dal Maso, M., Kulmala, M., Lehtinen, K., Mäkelä, J., Aalto, P., and O'Dowd, C.: Condensation and  
481 coagulation sinks and formation of nucleation mode particles in coastal and boreal forest boundary  
482 layers, *Journal of Geophysical Research: Atmospheres*, 107, 2002.
- 483 Dal Maso, M., Kulmala, M., Riipinen, I., Wagner, R., Hussein, T., Aalto, P. P., and Lehtinen, K. E.:  
484 Formation and growth of fresh atmospheric aerosols: eight years of aerosol size distribution data  
485 from SMEAR II, Hyytiälä, Finland, *Boreal Environment Research*, 10, 323, 2005.
- 486 Dal Maso, M., Hyvärinen, A., Komppula, M., Tunved, P., KERMINEN, V., Lihavainen, H., Viisanen, Y.,  
487 HANSSON, H. C., and Kulmala, M.: Annual and interannual variation in boreal forest aerosol particle  
488 number and volume concentration and their connection to particle formation, *Tellus B*, 60, 495-508,  
489 2008.
- 490 Eisele, F., and Hanson, D.: First measurement of prenucleation molecular clusters, *The Journal of*  
491 *Physical Chemistry A*, 104, 830-836, 2000.
- 492 Guo, S., Hu, M., Zamora, M. L., Peng, J., Shang, D., Zheng, J., Du, Z., Wu, Z., Shao, M., and Zeng, L.:  
493 Elucidating severe urban haze formation in China, *Proceedings of the National Academy of Sciences*,  
494 111, 17373-17378, 2014.

495 Huang, R.-J., Zhang, Y., Bozzetti, C., Ho, K.-F., Cao, J.-J., Han, Y., Daellenbach, K. R., Slowik, J. G., Platt,  
496 S. M., and Canonaco, F.: High secondary aerosol contribution to particulate pollution during haze  
497 events in China, *Nature*, 514, 218-222, 2014.

498 Jayaratne, E., Clifford, S., and Morawska, L.: Atmospheric Visibility and PM10 as Indicators of New  
499 Particle Formation in an Urban Environment, *Environmental science & technology*, 49, 12751-12757,  
500 2015.

501 Jayaratne, E. R., Ling, X., and Morawska, L.: Charging State of Aerosols during Particle Formation  
502 Events in an Urban Environment and Its Implications for Ion-Induced Nucleation, *Aerosol and Air  
503 Quality Research*, 16, 348-360, 2016.

504 Jeong, K.: Condensation of water vapor and sulfuric acid in boiler flue gas, ProQuest, 2009.

505 Kulmala, M., Vehkamäki, H., Petaja, T., Dal Maso, M., Lauri, A., Kerminen, V., Birmilli, W., and  
506 McMurry, P.: Formation and Growth Rates of Ultrafine Atmospheric Particles: A Review of  
507 Observations, *Journal of Aerosol Science*, 35, 143-176, 2004.

508 Kulmala, M., Petäjä, T., Mönkkönen, P., Koponen, I., Maso, M. D., Aalto, P., Lehtinen, K., and  
509 Kerminen, V.-M.: On the growth of nucleation mode particles: source rates of condensable vapor in  
510 polluted and clean environments, *Atmospheric Chemistry and Physics*, 5, 409-416, 2005.

511 Kulmala, M., Riipinen, I., Sipilä, M., Manninen, H. E., Petäjä, T., Junninen, H., Dal Maso, M., Mordas,  
512 G., Mirme, A., and Vana, M.: Toward direct measurement of atmospheric nucleation, *Science*, 318,  
513 89-92, 2007.

514 Kulmala, M., Petäjä, T., Nieminen, T., Sipilä, M., Manninen, H. E., Lehtipalo, K., Dal Maso, M., Aalto,  
515 P. P., Junninen, H., and Paasonen, P.: Measurement of the nucleation of atmospheric aerosol  
516 particles, *Nature protocols*, 7, 1651-1667, 2012.

517 Kulmala, M., Petäjä, T., Kerminen, V.-M., Kujansuu, J., Ruuskanen, T., Ding, A., Nie, W., Hu, M.,  
518 Wang, Z., and Wu, Z.: On secondary new particle formation in China, *Frontiers of Environmental  
519 Science & Engineering*, 10, 1-10, 2016.

520 Kulmala, M., Kerminen, V.-M., Petäjä, T., Aijun, D., and Wang, L.: Atmospheric Gas-to-Particle  
521 Conversion: why NPF events are observed in megacities?, *Faraday Discussions*, 2017.

522 Lehtinen, K. E., Korhonen, H., Maso, M., and Kulmala, M.: On the concept of condensation sink  
523 diameter, *Boreal environment research*, 8, 405-412, 2003.

524 Lehtinen, K. E., Dal Maso, M., Kulmala, M., and Kerminen, V.-M.: Estimating nucleation rates from  
525 apparent particle formation rates and vice versa: Revised formulation of the Kerminen–Kulmala  
526 equation, *J. Aerosol Sci.*, 38, 988-994, 2007.

527 Manninen, H., Franchin, A., Schobesberger, S., Hirsikko, A., Hakala, J., Skromulis, A., Kangasluoma, J.,  
528 Ehn, M., Junninen, H., and Mirme, A.: Characterisation of corona-generated ions used in a Neutral  
529 cluster and Air Ion Spectrometer (NAIS), *Atmospheric Measurement Techniques*, 4, 2767, 2011.

530 Manninen, H. E., Petaja, T., Asmi, E., Ripinen, I., Nieminen, T., Mikkila, J., Horrak, U., Mirme, A.,  
531 Mirme, S., Laakso, L., Kerminen, V., and Kulmala, M.: Long-term field measurements of charged and  
532 neutral clusters using Neutral cluster and Air Ion Spectrometer (NAIS), *Boreal Environment Research*,  
533 14, 591-605, 2009.

534 Manninen, H. E., Mirme, S., Mirme, A., Petäjä, T., and Kulmala, M.: How to reliably detect molecular  
535 clusters and nucleation mode particles with Neutral cluster and Air Ion Spectrometer (NAIS), *Atmos.*  
536 *Meas. Tech. Discuss*, 2016.

537 Massman, W.: A review of the molecular diffusivities of H<sub>2</sub>O, CO<sub>2</sub>, CH<sub>4</sub>, CO, O<sub>3</sub>, SO<sub>2</sub>, NH<sub>3</sub>, N<sub>2</sub>O,  
538 NO, and NO<sub>2</sub> in air, O<sub>2</sub> and N<sub>2</sub> near STP, *Atmos. Environ.*, 32, 1111-1127, 1998.

539 Mirme, A., Tamm, E., Mordas, G., Vana, M., Uin, J., Mirme, S., Bernotas, T., Laakso, L., Hirsikko, A.,  
540 and Kulmala, M.: A wide-range multi-channel Air Ion Spectrometer, *Boreal Environmental Research*,  
541 12, 247-264, 2007.

542 Salma, I., Borsós, T., Weidinger, T., Aalto, P., Hussein, T., Dal Maso, M., and Kulmala, M.: Production,  
543 growth and properties of ultrafine atmospheric aerosol particles in an urban environment, *Atmos.*  
544 *Chem. Phys.*, 11, 1339-1353, 2011.

545 Seinfeld, J. H., and Pandis, S. N.: *Atmospheric chemistry and physics*. Hoboken, NJ: Wiley, 2006b.

546 Wang, M., Zhu, T., Zheng, J., Zhang, R., Zhang, S., Xie, X., Han, Y., and Li, Y.: Use of a mobile  
547 laboratory to evaluate changes in on-road air pollutants during the Beijing 2008 Summer Olympics,  
548 Atmospheric Chemistry and Physics, 9, 8247-8263, 2009.

549 Wehner, B., Wiedensohler, A., Tuch, T., Wu, Z., Hu, M., Slanina, J., and Kiang, C.: Variability of the  
550 aerosol number size distribution in Beijing, China: New particle formation, dust storms, and high  
551 continental background, Geophysical Research Letters, 31, 2004.

552 Wu, Z., Hu, M., Liu, S., Wehner, B., Bauer, S., Wiedensohler, A., Petäjä, T., Dal Maso, M., and  
553 Kulmala, M.: New particle formation in Beijing, China: Statistical analysis of a 1-year data set, Journal  
554 of Geophysical Research: Atmospheres, 112, 2007.

555 Wu, Z., Hu, M., Yue, D., Wehner, B., and Wiedensohler, A.: Evolution of particle number size  
556 distribution in an urban atmosphere during episodes of heavy pollution and new particle formation,  
557 Science China Earth Sciences, 54, 1772, 2011.

558 Xiao, S., Wang, M., Yao, L., Kulmala, M., Zhou, B., Yang, X., Chen, J., Wang, D., Fu, Q., and Worsnop,  
559 D.: Strong atmospheric new particle formation in winter in urban Shanghai, China, Atmospheric  
560 Chemistry and Physics, 15, 1769-1781, 2015.

561 Xue, Y., Zhou, Z., Nie, T., Pan, T., Qi, J., Nie, L., Wang, Z., Li, Y., Li, X., and Tian, H.: Exploring the  
562 Severe Haze in Beijing During December, 2015: Pollution Process and Emissions Variation, Huan jing  
563 ke xue= Huanjing kexue/[bian ji, Zhongguo ke xue yuan huan jing ke xue wei yuan hui" Huan jing ke  
564 xue" bian ji wei yuan hui.], 37, 1593, 2016.

565 Yu, H., Zhou, L., Dai, L., Shen, W., Dai, W., Zheng, J., Ma, Y., and Chen, M.: Nucleation and growth of  
566 sub-3 nm particles in the polluted urban atmosphere of a megacity in China, Atmospheric Chemistry  
567 and Physics, 16, 2641-2657, 2016.

568 Yue, D., Hu, M., Zhang, R., Wang, Z., Zheng, J., Wu, Z., Wiedensohler, A., He, L., Huang, X., and Zhu,  
569 T.: The roles of sulfuric acid in new particle formation and growth in the mega-city of Beijing,  
570 Atmospheric Chemistry and Physics, 10, 4953-4960, 2010.



571 Zhang, Q., Stanier, C., Canagaratna, M., Jayne, J., Worsnop, D., Pandis, S., and Jiminez, J.: Insights  
572 into the Chemistry of New Particle Formation and Growth Events in Pittsburgh Based on Aerosol  
573 Mass Spectrometry, *Environmental Science and Technology*, 38, 4797-4809, 2004.

574 Zhang, R., Khalizov, A., Wang, L., Hu, M., and Xu, W.: Nucleation and growth of nanoparticles in the  
575 atmosphere, *Chemical Reviews*, 112, 1957-2011, 2011.

576 Zhibin, W., Min, H., Zhijun, W., and Dingli, Y.: Reasearch on the Formation Mechanisms of New  
577 Particles in the Atmosphere, *Acta Chimica Sinica*, 71, 519-527, 2013.

578

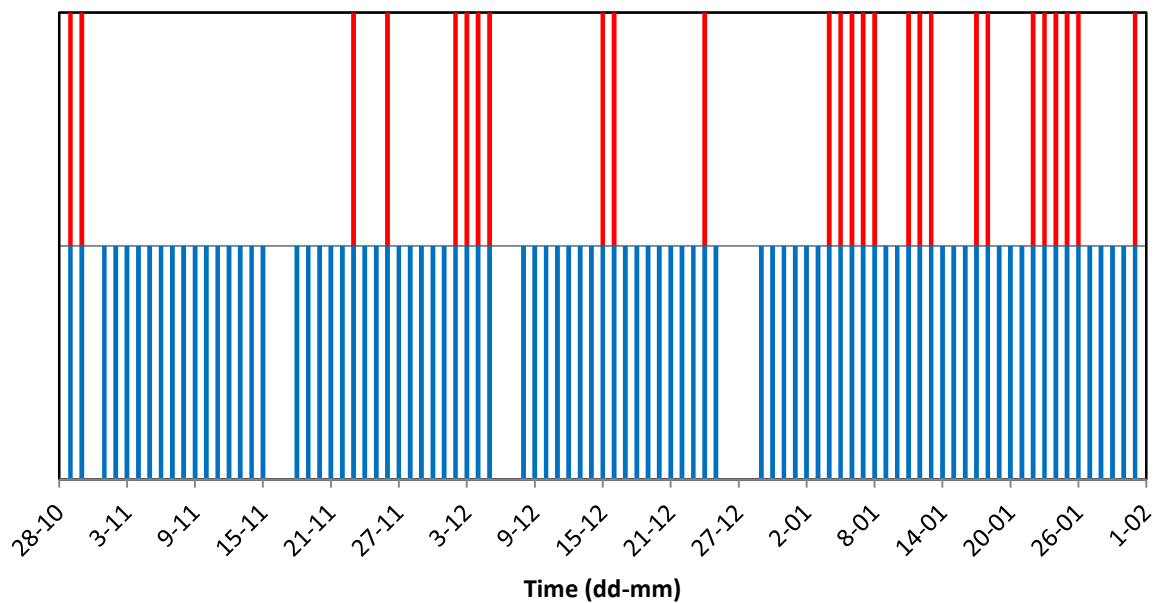
579

580

### Figures

581

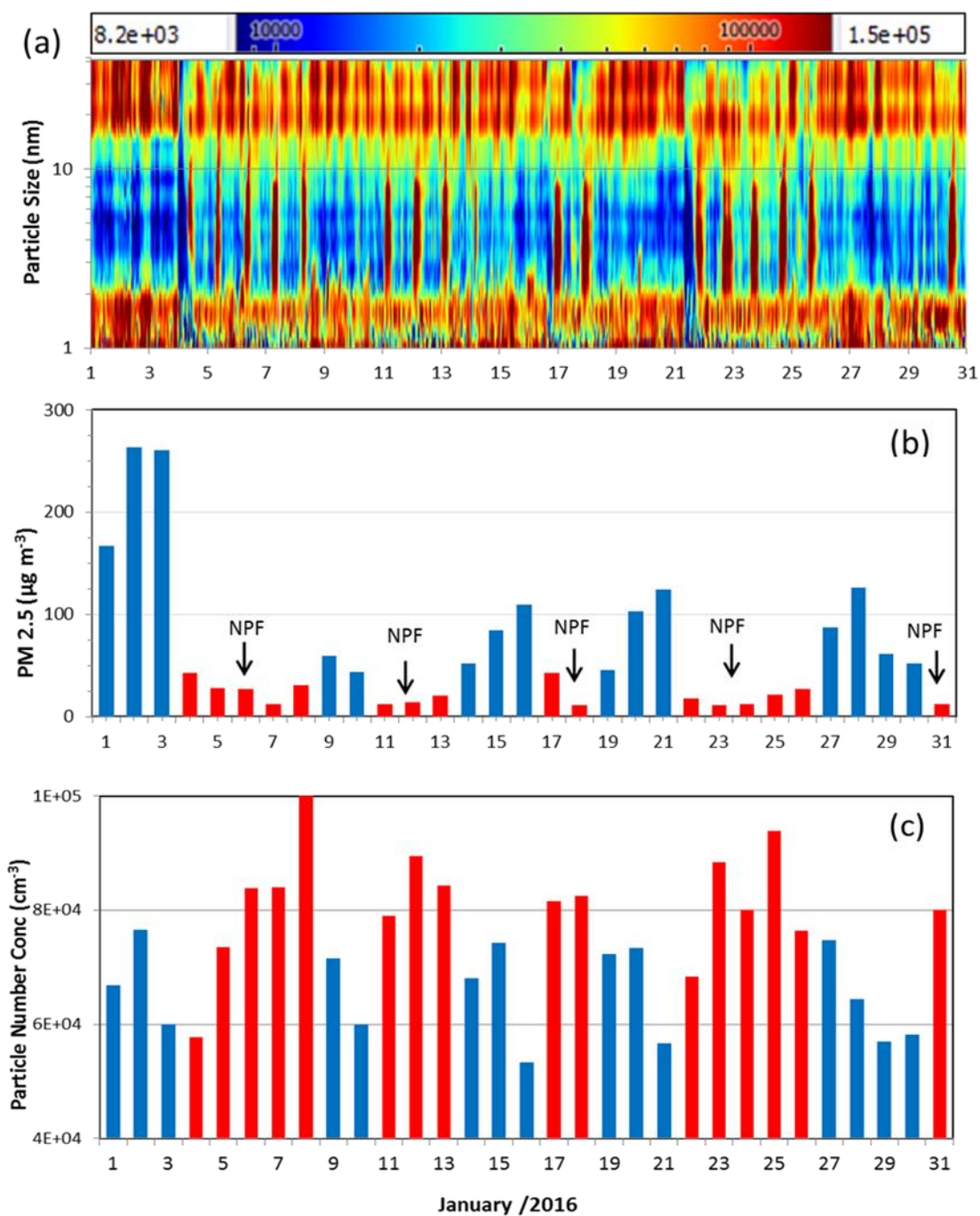
582



583

584 Figure 1: Summary of observational days (lower panel in blue) and days with NPF events (upper  
585 panel in red).

586



587

588

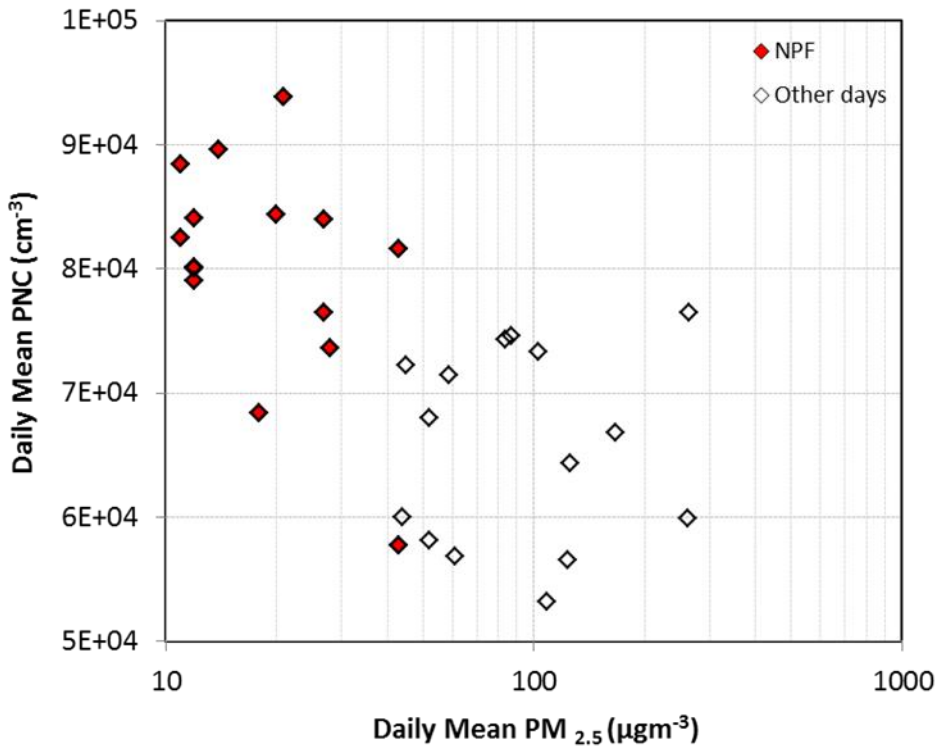
589 Figure 2: Daily values for January 2016: (a) NAIS Spectrogram of PNC on a particle size–time diagram

590 (b) mean  $\text{PM}_{2.5}$  concentration from the TEOM and (c) mean PNC in the size range 2 – 42 nm

591 from the NAIS. In (a), the units of PNC are  $\text{cm}^{-3}$ . Data below 2.0 nm should be treated with

592 caution due to instrumentation limitations as described in the text. In (c), the red and blue

593 bars represent the NPF days and other days, respectively.

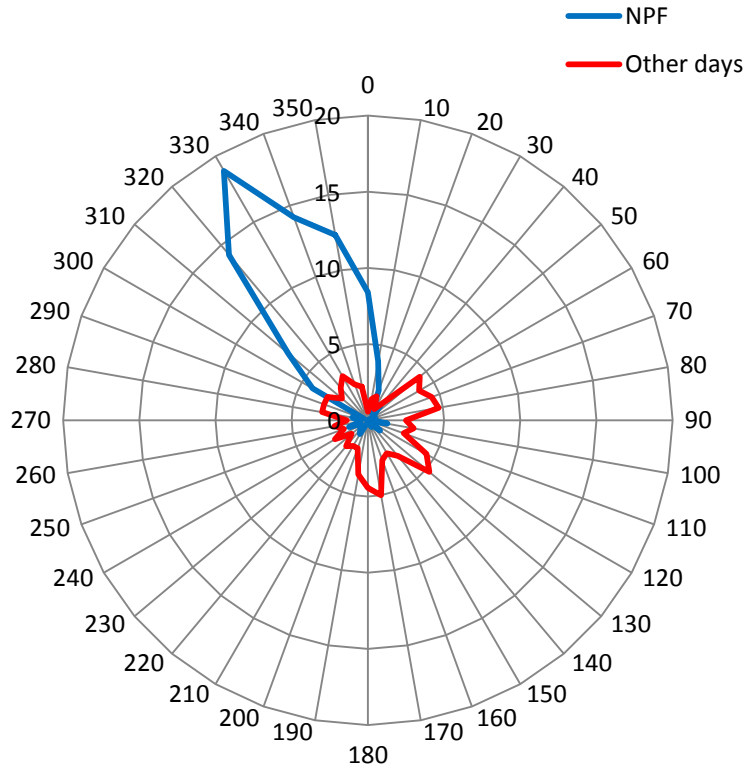


594

595

596 Figure 3: Daily mean PNC vs PM<sub>2.5</sub> for NPF days (filled markers) and other days (open markers) during  
 597 January 2016.

598



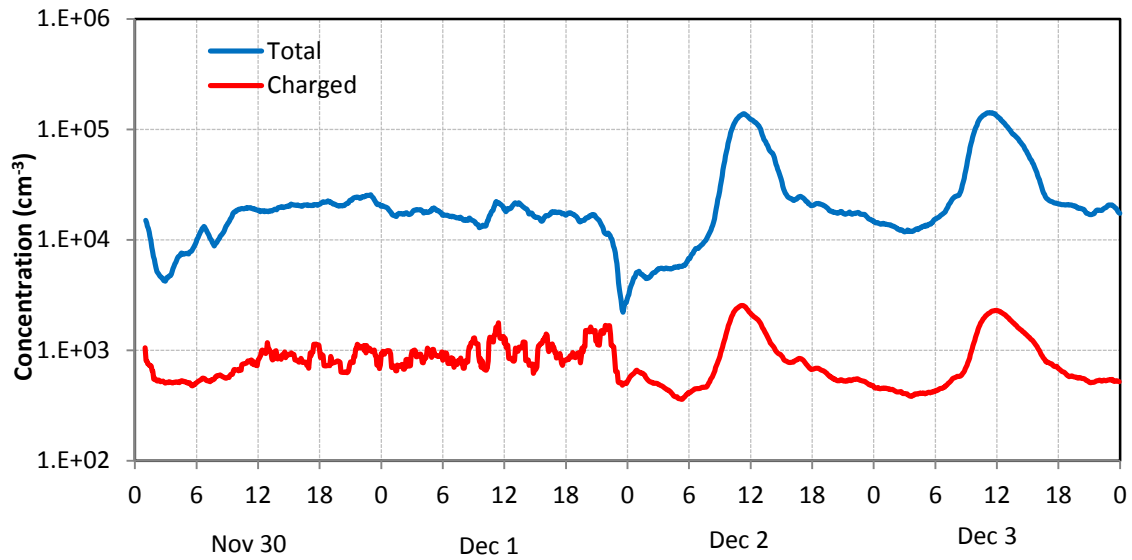
599

600

601 Figure 4: The wind direction rose for NPF days and other days during January. The radial scale

602 indicates percentages of time.

603



604

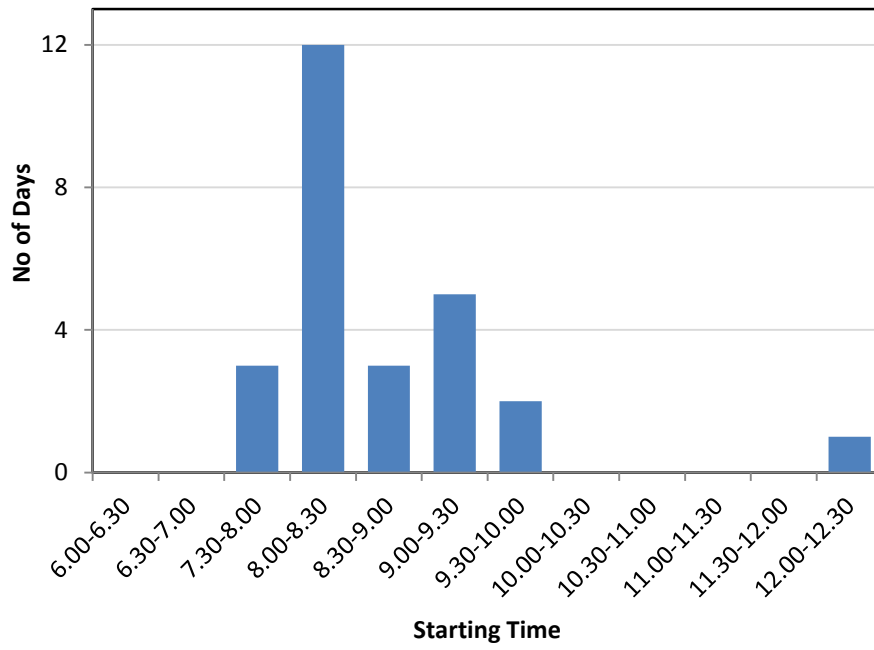
605

606 Figure 5: Time series of total and charged particles during the period 30 Nov to 3 Dec as measured

607 by the NAIS. 30 Nov and 1 Dec were haze days while two NPF events occurred on 2 and 3

608 Dec.

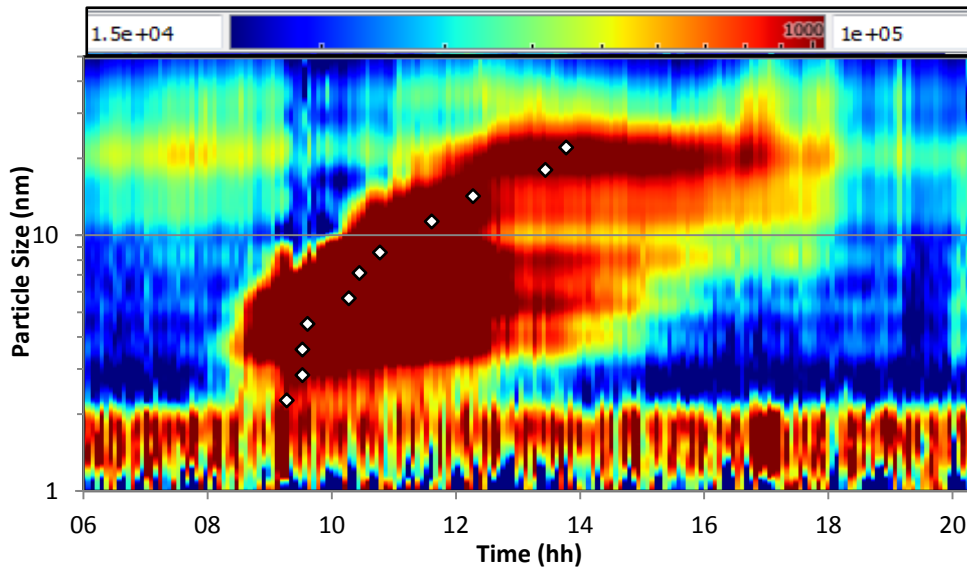
609



610

611 Figure 6: Distribution of the start times of the NPF events, classified into 30 min bins.

612



613

614 Figure 7: NAIS spectrogram of the NPF event that occurred on 29<sup>th</sup> October. The clear banana shape

615 indicates strong particle growth. The markers show the median particle size at each time.

616 The units of PNC are  $\text{cm}^{-3}$ . Data below 2.0 nm should be treated with caution due to

617 instrumentation limitations as described in the text.

618



619

**Tables**

620

621

622

Table 1: Summary of the observational days.

| Month           | Total Days | Data Available Days | NPF Days :<br>$dN/dt > 15000 \text{ cm}^{-3} \text{ h}^{-1}$ |
|-----------------|------------|---------------------|--|
| October (28-31) | 4          | 2                   | 2  |
| November (1-30) | 30         | 28                  | 2  |
| December (1-31) | 31         | 26                  | 6  |
| January (1-31)  | 31         | 31                  | 16   |
| Total           | 96         | 87                  | 26   |

623

624 Table 2: Mean and peak values of neutral and charged particle concentrations during the various  
625 types of days and events. The associated uncertainties in the values are up to 20%. The % column  
626 shows the charged/total percentages.

627

628

|                    | Particles (cm <sup>-3</sup> ) |                     |      |
|--------------------|-------------------------------|---------------------|------|
|                    | Neutral                       | Charged             | %    |
|                    | (x10 <sup>4</sup> )           | (x10 <sup>4</sup> ) |      |
| Normal Days (mean) | 5.6                           | 0.9                 | 14.5 |
| NPF Days (mean)    | 7.6                           | 0.8                 | 10.1 |
| NPF Events (peak)  | 22.5                          | 1.3                 | 5.6  |
| Haze Days (mean)   | 4.8                           | 1.9                 | 28.6 |
| Haze Events (peak) | 11.7                          | 2.9                 | 20.1 |

629

630 Table 3: Summary of mean and range of parameters calculated for the NPF events observed.

| Parameter                                     | Mean                 | Range                        |
|---|----------------------|------------------------------|
| Starting Time of NPF                          | 8.45 am              | 7.30 am - 12.30 pm           |
| Condensation sink ( $s^{-1}$ )                | $4.2 \times 10^{-3}$ | $(2.3 - 5.7) \times 10^{-3}$ |
| Coagulation sink ( $s^{-1}$ )                 | $7.2 \times 10^{-4}$ | $(3.9 - 9.7) \times 10^{-4}$ |
| Formation rate ( $J_2$ ) ( $cm^{-3} s^{-1}$ ) | 26                   | 12 - 38                      |
| Growth rate ( $nm h^{-1}$ )                   | 3.5                  | 0.5 - 9.0                    |

631